ACS APPLIED MATERIALS & INTERFACES

Research Article

www.acsami.org

Correlating Li/O_2 Cell Capacity and Product Morphology with Discharge Current

Lucas D. Griffith,[†] Alice E.S. Sleightholme,[†] John F. Mansfield,[‡] Donald J. Siegel,[§] and Charles W. Monroe*,[†]

[†]Department of Chemical Engineering, 2300 Hayward St., University of Michigan, Ann Arbor Michigan 48109, United States

[‡]Electron Microbeam Analysis Laboratory, 2800 Plymouth Road, University of Michigan, Ann Arbor, Michigan 48109, United States

[§]Department of Mechanical Engineering, 2350 Hayward St., University of Michigan, Ann Arbor, Michigan 48109, United States

Supporting Information

ABSTRACT: The discharge rate is critical to the performance of lithium/oxygen batteries: it impacts both cell capacity and discharge-phase morphology, and in so doing may also affect the efficiency of the oxygen-evolution reaction during recharging. First-discharge data from tens of Li/O_2 cells discharged across four rates are analyzed statistically to inform these connections. In the practically significant superficial current-density range of 0.1 to 1 mA cm^{-2}, capacity is found to fall as a power law, with a Peukert's-law exponent of 1.6 ± 0.1. X-ray diffractometry confirms the dominant presence of crystalline Li_2O_2 in the discharged electrodes. A completely air-free sample-transfer technique was developed to implement scanning electron microscopy (SEM) of the discharge product. SEM imaging of electrodes with near-average capacities provides statistically significant measures of the shape and size variation of electrodeposited Li_2O_2 particles with respect to discharge current. At lower rates, typical "toroidal" particles are observed that are well approximated as cylindrical structures, whose average radii remain relatively constant as discharge rate increases, whereas their average heights decrease. At the highest rate studied, air-free SEM shows that particles take needle-like shapes rather than forming the nanosheets or compact films described elsewhere. Average particle volumes decrease with current while particle surface-to-volume ratios increase dramatically, supporting the notion that Li_2O_2 grows by a locally mass-transfer-limited nucleation and growth mechanism.

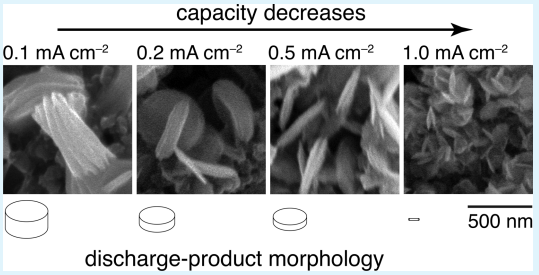

KEYWORDS: *lithium−oxygen batteries, rate performance, morphology, Peukert's law, nucleation and growth*

1. INTRODUCTION

Limited range and high cost currently prevent the widespread implementation of battery-electric vehicles.[1] Both of these challenges could be addressed by realizing an efficient, cyclable lithium/oxygen (Li/O_2) battery. For automotive applications, the high theoretical specific energy of Li/O_2 chemistry makes it attractive as a possible alternative to lithium-ion chemistries.[2,3]

Although relatively high cell capacities have been obtained on the laboratory scale,[4] a number of significant barriers, including short cycle life and low charging efficiency, must be overcome for Li/O_2-battery technology to become practical.[2] Addressing such challenges demands a deeper understanding of the energy storage and retrieval mechanisms in the porous positive electrode. The present investigation aims to shed light on the operating mechanisms of nonaqueous Li/O_2 cells by examining how cell capacity and discharge-product morphology depend on the discharge rate.

Nonaqueous Li/O_2 cells ideally discharge by the reduction of oxygen to form an oxygenated lithium species at the positive electrode,[5] which substantial literature confirms is mostly lithium peroxide (Li_2O_2).[6−10] During an ideal recharge process, the Li_2O_2 should decompose electrochemically, returning lithium and oxygen to their original states. Even when taking the masses of the electrode substrate and the oxygen added to the peroxide into account, Li/O_2 cells exhibit theoretical specific energies 3−5 times greater than conventional lithium-ion cells.[4] This benefit owes both to the exchange of intercalation-compound-laden positive electrodes for lighter gas-diffusion electrodes and to the replacement of the graphite negative electrode with energy-dense metallic Li.

There are many reports of discharged Li/O_2 cells whose positive electrodes contain electrodeposited Li_2O_2 particles with a "toroid"-like morphology; these toroids typically have characteristic dimensions of hundreds of nanometers.[8,9,11−14] Because Li_2O_2 is a bulk insulator that in principle should prevent electrons from traveling such distances,[15] the observations suggest that unconventional electron-transport pathways or diffusion of intermediates may play roles in the discharge process. For example, mechanisms by which charge could travel through amorphous Li_2O_2[16] or across crystalline Li_2O_2 via its surface,[17] grain boundaries,[18] or defects in its bulk[15] have been proposed. Studies also show that the

Received: January 20, 2015
Accepted: March 16, 2015
Published: March 16, 2015

DOI: 10.1021/acsami.5b00574
ACS Appl. Mater. Interfaces 2015, 7, 7670−7678

morphology of Li_2O_2 deposited on a porous-carbon positive electrode can change when additives are incorporated.[13,19] Adams et al. provided a detailed set of hypotheses to rationalize how discharge-product morphology depends on discharge rate.[8] They observed that the Li_2O_2 morphology transitioned from toroids to a compact film as the discharge-current density increased; they also noted that capacity remained relatively stable until a critical rate, above which the capacity substantially deteriorated.

Although a few studies highlight challenges related to the rate performance of Li/O_2 cells and cell design, research in this direction has received relatively little attention.[4] For example, Adams et al.[20] fabricated a bipolar-plate battery design aimed at meeting various goals set by the U.S. Advanced Battery Consortium;[21] their testing, which explored discharge currents up to 4 mA cm^{-2} (per superficial electrode area), suggests that current densities of the order of 1 mA cm^{-2} could be required in practice. Lu et al. fabricated extremely thin electrodes, with the aims of mitigating mass-transport limitations and allowing higher current densities.[22] They discharged their cells at up to 0.76 mA cm^{-2} of superficial positive-electrode area. Jung et al. achieved one hundred cycles at rates of ±1 mA cm^{-2} by limiting the depth of discharge, and also demonstrated comparable capacity at ±3 mA cm^{-2}.[23]

A viable vehicular battery must retain its performance at higher rates. Consequently, more work is needed to understand the properties of Li/O_2 batteries operated at high current densities. In addition to the aforementioned effects on capacity and Li_2O_2 morphology, there is evidence that higher rates of discharge result in lower overpotentials during recharging.[8,9] Hence, discharge rate may ultimately control not only the capacity but also the round-trip efficiency of a Li/O_2 battery. This paper explores the capacity of Li/O_2 cells and morphology of Li_2O_2 at the end of first discharge in the practically significant 0.1 to 1 mA cm^{-2} superficial current-density range. Cell capacity is found to fall with a power-law dependence on current across these rates. Understanding this response, which can be associated with a Peukert's-law[24] exponent of 1.6 ± 0.1, could aid the engineering of cells with better rate performance.

More than 60 separate first-discharge experiments were performed across four rates. Electrodes exhibiting near-average capacity at a given rate were characterized using X-ray diffractometry (XRD) and scanning electron microscopy (SEM). Air-free sample-transfer techniques were used to implement XRD of representative electrodes, minimizing any changes to the discharge-product morphology incurred by air exposure. A novel sample-transfer technique was developed for SEM that allows airtight argon-filled sample holders to be opened inside the microscope chamber after vacuum is drawn. Micrographs from representative cells are used to develop quantitative measures of how the sizes and shapes of deposited Li_2O_2 particles vary with control conditions.

The observed power-law dependence of discharge capacity on discharge rate is consistent with a macroscopic oxygen-transport limitation that lowers utilization of the porous positive electrode, similar to the mechanism described by Nanda et al.[25] Particle volumes are also found to fall dramatically with rate, whereas their surface-to-volume ratios rise. Thus, Li_2O_2 appears to be produced by a nucleation-and-growth process over the range of currents studied, supporting the notion that particle growth is transport-limited on a microscopic scale, as well as on a macroscopic scale.[26] Particle shapes could be determined by voltage-dependent surface energetics, consistent with a deposition mechanism involving direct charge transfer. Alternatively, the particle-growth process could be mediated by chemical precipitation of a neutral reaction intermediate, whose local supersaturation in the liquid rises with discharge rate.

2. EXPERIMENTAL SECTION

2.1. Materials. Electrolytic solutions were prepared by dissolving lithium bis(trifluoromethane sulfonyl)imide (99.95%, Sigma-Aldrich, U.S.A.) to 1 M concentration in dimethoxyethane (DME, 99.5% anhydrous, Sigma-Aldrich, U.S.A.), which was dried over 4 Å molecular sieves (Fisher Scientific, U.S.A.). Each electrochemical cell comprised a 0.75 mm thick, 18 mm diameter Li disk negative electrode (99.9%, Alfa Aesar, U.S.A.), a 0.65 mm thick, 18 mm diameter glass-fiber separator (EL-CELL GmbH, Germany), and an 18 mm diameter porous-carbon positive electrode (SIGRACET GDL 24 BC, Ion Power, Inc., U.S.A.). Both electrodes were cut from larger sheets of material using a steel punch. The average positive-electrode mass was 0.0265 g; its porosity, 0.8 (as per supplier); its thickness, 235 ± 20 μm (as per supplier); and its specific surface area, 13.3 ± 0.2 m^2 g^{-1} (measured by N_2 physisorption with a Micromeritics ASAP 2010 analyzer employing the Brunauer–Emmett–Teller isotherm). Positive electrodes and separators were dried under vacuum at 110 °C for 12 h to remove residual water.

2.2. Electrochemical Cell Assembly. ECC-AIR metal–oxygen electrochemical test cells were purchased from EL-CELL GmbH (Germany). Cells were assembled in an Omnilab glovebox (Vacuum Atmospheres, U.S.A.) with an Ar atmosphere (99.998%, Cryogenic Gases, U.S.A.) containing less than 1 ppm of O_2 and less than 1 ppm of H_2O. To prepare cells for discharge experiments, the vacuum-dried glass-fiber separator and porous-carbon positive electrode were soaked in the electrolytic solution for ∼1 min, after which the carbon electrode was sandwiched between the separator and a perforated stainless-steel current collector. The wetted, stacked assembly was then slid into a cylindrical polyether ether ketone (PEEK) sleeve, leaving the soaked glass-fiber surface exposed. The Li foil was subsequently placed onto the glass-fiber surface, after which the entire assembly within the PEEK sleeve was inserted into a stainless-steel cell base, which acted as the current collector for the negative electrode. The base was then sealed using an electrically isolated stainless-steel cap containing a spring-loaded, hollow piston that applied reproducible pressure on the stacked assembly; the spring was gold plated to provide electrical contact with the positive current collector. An opening in the piston allowed distribution of gases to the positive electrode through the perforated plate. To initiate each test, a Series 4000 battery tester (Maccor, U.S.A.) was used to hold the assembled, sealed cell at open circuit until the rate of voltage change was observed to fall below 2 mV h^{-1}, typically requiring a hold period of 10–15 h. (Figure S1 of the Supporting Information provides a few typical data sets for the voltage transients during the open-circuit holds.) Throughout the test a series HP702 pressure regulator (Harris Specialty Gas, U.S.A.) was used to maintain the pressure of stagnant O_2 gas (99.993%, Cryogenic Gases, U.S.A.) at 1 bar gauge. Oxygen was supplied to the cells via a gas manifold consisting of Swagelok steel tubing. Each cell was fitted with a three-way valve to allow the lines to be purged prior to each test. Individual cells were connected to the gas manifold with about 30 cm of 1/16 in. OD PTFE tubing (McMaster Carr, U.S.A.), which was used instead of the PEEK tubing supplied by EL-CELL to prevent permeation by ambient water and oxygen. After the ∼12 h initial equilibration period, cells were discharged at constant current densities of 0.1, 0.2, 0.5, or 1.0 mA cm^{-2} (superficial) until the voltage reached a lower cutoff of 2.0 V. Every cell was purged with Ar gas and sealed immediately after first discharge. (Control experiments were also run, by holding assembled cells at zero current under 1 bar gauge O_2 pressure for 24 h.)

2.3. Ex Situ Characterization. After being discharged, cells were disassembled in the glovebox. Carbon electrodes were removed and rinsed with ∼10 mL of sieved DME, after which they were dried at room temperature under vacuum in the glovebox antechamber for 20

DOI: 10.1021/acsami.5b00574
ACS Appl. Mater. Interfaces 2015, 7, 7670–7678

min and returned to the main chamber. After removal, each electrode was sectioned with steel scissors into eight smaller samples for analysis.

XRD samples were prepared in the glovebox by placing sections of the discharged electrodes in an airtight sample holder with a Be window (2455-SH-001, Rigaku, Japan). Diffraction patterns were gathered by a Rotaflex (40 kV, 100 mA) diffractometer (Rigaku, Japan) with a Cu source, using continuous scan at 0.75° min^{-1} in 2θ mode.

SEM samples were prepared in the glovebox and transferred to the microscope chamber using an airtight holder designed and fabricated in house, to prevent exposure of samples to ambient air prior to micrograph acquisition. The sample holder comprised a "clamshell" design with a hinged Al cap atop a hollow Al cylindrical base that also served as a pin stub. After samples were anchored on double-sided Cu tape inside the hollow cylindrical cavity, the cap was wedged tightly in contact with an O-ring on the lip of the base by a U-shaped Be/Cu-alloy spring clamp attached in opposition to the hinge. For transfer to the SEM facility, the clamped sample holder was placed inside an airtight storage container in the glovebox. Once removed from the glovebox and transported to the microscope, the container was opened and the clamped sample holder was placed inside the SEM chamber. The spring clamp was affixed to an interior wall of the chamber with a taut wire, allowing it to be removed by translation of the sample stage after the chamber was closed and vacuum was drawn. The hinged cap was also affixed to an interior wall of the chamber with a second wire. After removal of the clamp, 180° rotation of the stage allowed the hinged cap to be opened, revealing the sample. Schematic diagrams of the sample holder and spring clamp are provided in the Supporting Information (Figure S2). SEM was performed with a FEI Nova NanoLab microscope (5 kV accelerating voltage, 98 pA). SEM images were gathered using a 50 ns acquisition time and integrating 64 frames. Particle dimensions were analyzed with SPIP software.

3. RESULTS

3.1. First-Discharge Capacity vs Rate. More than 60 independent cells were assembled and discharged at four rates to establish the average capacity. Approximately two out of every three discharge curves met all of the following criteria for a successful discharge: monotonically decreasing potential for the entire discharge period; clear "sudden death" of voltage at the end of discharge (i.e., a cell voltage vs capacity slope within two standard deviations of the mean for that rate at the cutoff voltage), and a first-discharge capacity within two standard deviations of the mean for that rate. It should be noted that these criteria are quite strict: nonmonotonic domains and poorly comparable sudden-death behavior are commonly observed in the literature.[9,27−29]

Figure 1 shows the potential vs capacity curves for all successful discharges at each discharge rate studied. Averages and standard deviations of the first-discharge capacities are respectively shown by vertical solid and dashed lines in each plot. The figure shows 8 successful discharges at 0.1 mA cm^{-2}, 12 at 0.2 mA cm^{-2}, 9 at 0.5 mA cm^{-2}, and 9 at 1 mA cm^{-2}. Significant statistical variation was observed in both the first-discharge capacity and overpotential. Figure 2 shows the cell potential at 50% depth of discharge (DOD) vs discharge rate for all successful discharges, along with the averages and standard deviations. Following an analysis similar to that of Viswanathan et al.,[30] these yield a Tafel slope of 11 ± 1 V^{-1} and an exchange-current density of 7 ± 3 $\mu A\ cm^{-2}$ (superficial).

As far as we know, no prior reports have quantified the inherent random variability of Li_2O_2 cells. The stochastic variation is measured by the standard deviations of capacity and mid-discharge cell potential, which both increase as the discharge rate rises. Large mean overpotentials could arise from sluggish reaction kinetics[31] or diffusion limitations;[32]

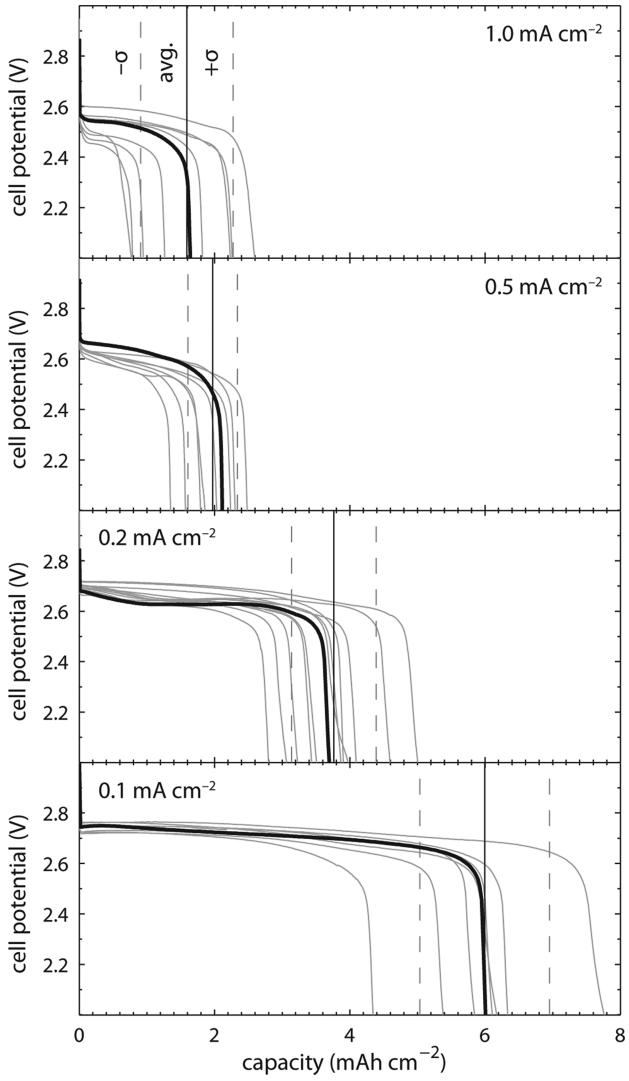

Figure 1. Dependence of potential on capacity (per superficial area) for lithium−oxygen cells discharged at 1.0, 0.5, 0.2, and 0.1 mA cm^{-2}. Vertical solid lines show the average discharge capacity; vertical dashed lines indicate its standard deviation. The black curves correspond to the discharges of cells used for SEM and XRD.

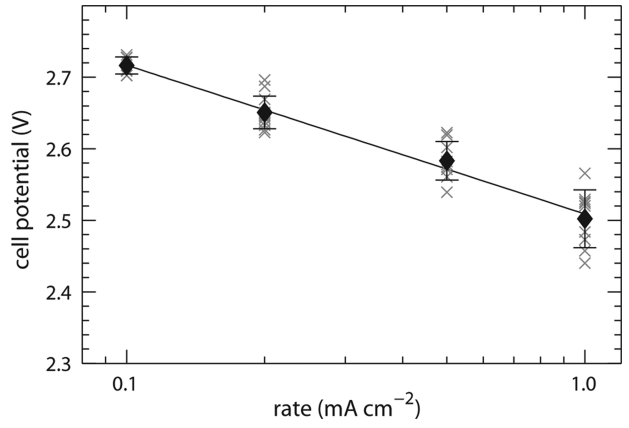

Figure 2. Cell potential at 50% depth-of-discharge with respect to rate. Diamonds show the mean potential, and error bars show one standard deviation.

DOI: 10.1021/acsami.5b00574
ACS Appl. Mater. Interfaces 2015, 7, 7670−7678

variation in the overpotential could owe to the inherent variability of pore-surface area in the electrodes.

Peukert's law is an empirical expression that describes the relationship between a battery cell's discharge current and discharge duration as a power law.[24] In the present context, it is convenient to express Peukert's law in terms of the areal capacity q_{total} (superficial basis) and the superficial discharge-current density i, as

$$\ln\left(\frac{q_{total}}{q_{ref}}\right) = (1-k)\ln\left(\frac{i}{i_{ref}}\right) \quad (1)$$

where k is the Peukert exponent, i_{ref} is a reference current density, and q_{ref} is the areal capacity at i_{ref}. If the full capacity of a battery system were available at all discharge rates, its Peukert exponent would be 1. The second law of thermodynamics requires that $k > 1$; the specific exponent observed for a given cell chemistry and geometry is commonly acknowledged to arise from the combination of dissipative processes that limits capacity (ohmic loss, mass-transport limitations, kinetic resistances, etc.).[33] Peukert's law fits the observed rate dependence of capacity in some current ranges for lead/acid and lithium-ion batteries.[24,34−36] The lead/acid system, which may be most comparable to Li/O_2 because it also operates by a precipitation-dissolution mechanism, satisfies Peukert's law well over a broad current range, with an exponent of 1.4.[34]

Figure 3 presents the areal discharge capacities with respect to discharge rate for the successfully discharged Li/O_2 cells.

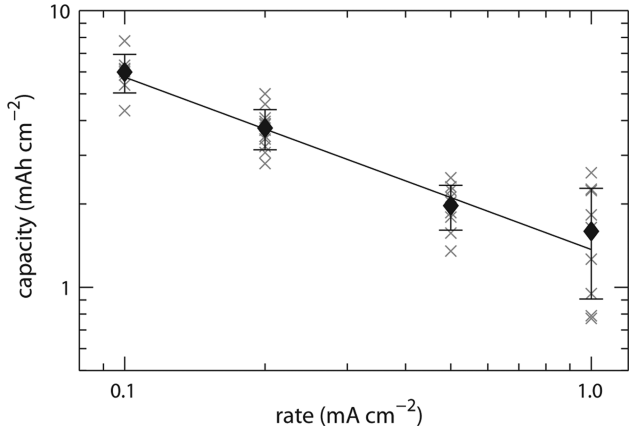

Figure 3. Capacity falls as a power law with respect to discharge rate. Capacity per geometric electrode area achieved at the 2 V cutoff potential as a function of discharge-current density on a geometric-area basis. Diamonds show the average discharge capacity, and error bars show one standard deviation.

The capacities observed during the Li/O_2-cell discharges follow a power-law dependence on the discharge current, yielding a Peukert exponent of 1.6 ± 0.1 and reference capacity of 1.4 ± 0.2 mAh cm^{-2} at 1 mA cm^{-2}.

3.2. Discharge-Product Identification. XRD patterns from representative positive electrodes at each discharge rate are shown in Figure 4. Because variability in capacity could arise from side reactions or poor selectivity for Li_2O_2, XRD was used to confirm the presence of the Li_2O_2 discharge product. (Note that because XRD can only identify crystalline phases, any amorphous compounds were not detected.) Although past studies have identified products from side reactions with the solvent,[6] lithium salt,[37] and positive-electrode substrate,[38] the

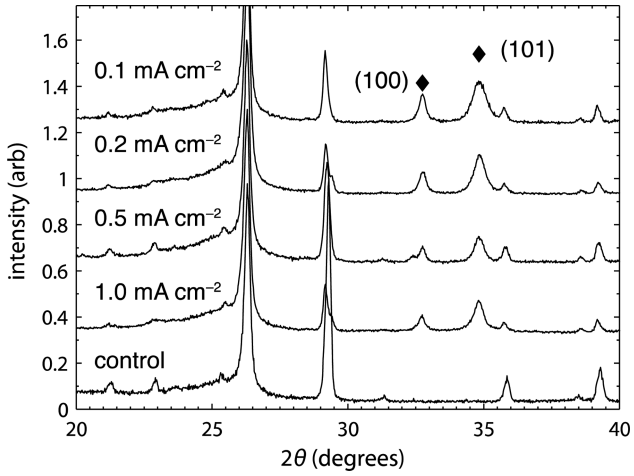

Figure 4. Diffraction patterns of representative positive electrodes at all four discharge rates exhibit peaks that correspond to the (100) and (101) reflections of Li_2O_2.

only consistently apparent diffraction peaks unique to the discharged electrodes studied here correspond to crystalline Li_2O_2. Evidence of trace crystalline LiOH, which manifests as an apparent small second peak adjacent to the Li_2O_2 (100) peak, was seen in some cases; in Figure 4, for example, trace LiOH affects the diffraction pattern of the electrode discharged at 0.5 mA cm^{-2}. In every XRD pattern, the height of the peak corresponding to the Li_2O_2 (100) plane is slightly larger relative to the (101) peak than would be expected for large crystallites of pure Li_2O_2. The broadening of the peaks associated with Li_2O_2 suggests a crystallite size of about 20 nm, which was constant across all rates. No signal for crystalline Li_2CO_3 or Li_2O was observed in any XRD sample.

3.3. Discharge-Product Morphology. In hopes of isolating the effect of applied current on discharge-product morphology, microscopy was performed on electrodes from cells exhibiting near-average capacity at each of the discharge rates. Figure 5 shows SEM images of Li_2O_2 particles gathered at end-of-discharge from representative cells at each of the discharge rates, whose corresponding discharge curves are highlighted in Figure 1. During all measurements, the SEM beam was destructive to the Li_2O_2; owing to their smaller sizes, the Li_2O_2 particles deposited at higher rates were destroyed more quickly. Degradation of the Li_2O_2 particles during imaging was mitigated by using relatively fast scan rates and integrating over 64 scans, as described in the Experimental Section.

In general, the micrographs in Figure 5 show that the Li_2O_2 deposits take "disk-like" cylindrical shapes at the lower rates, whereas "needle-like" particles form at the highest rate. Note that the characteristic Li_2O_2 discharge-product shape observed at low rates is often referred to in the literature as "toroidal," as mentioned in the Introduction.[9,11−13,20] The shapes observed in the present work were consistent with those seen by other researchers, but the larger particles are referred to as "disks" or "cylinders" here because (1) none of the particles was observed to contain a central void space and (2) asserting that particles are "toroids" could imply a particular particle-growth mechanism in which nucleation progresses to propagation via a ring-shaped primary structure, rather than via a linear (needle-shaped) or hemispherical primary structure. At the lowest rate, 0.1 mA cm^{-2}, the axial dimension of the Li_2O_2 disks is largest.

DOI: 10.1021/acsami.5b00574
ACS Appl. Mater. Interfaces 2015, 7, 7670−7678

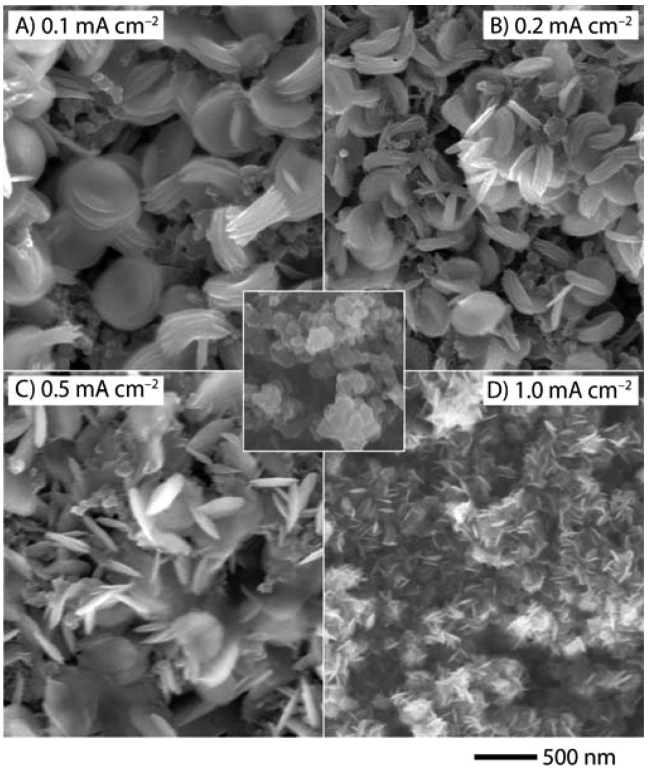

Figure 5. Scanning electron micrographs of Li_2O_2 formed at various discharge rates (100,000× magnification). The inset at the center of the image shows a control electrode at similar magnification.

At the two lowest rates, 0.1 and 0.2 mA cm^{-2}, parallel stria spaced by about 20 nm can be discerned on the curved faces of the particles. As the rate increases from 0.1 to 0.5 mA cm^{-2}, the particle heights decrease, whereas their radii stay relatively constant; the aspect ratio rises with current. The height and radius trends reverse for the particles formed at 1 mA cm^{-2}; if these particles are considered to be cylindrical rods as well, then the typical aspect ratio is dramatically smaller than the aspect ratios at lower currents due to the qualitative change in shape.

SPIP image-analysis software was used to determine average dimensions of the Li_2O_2 particles formed at each discharge rate. Multiple SEM images were processed to identify at least 25 particles from each carbon electrode at each discharge rate, for which average cylinder heights and diameters were recorded. Table 1 reports the diameter, height, surface-to-volume ratio, and number of particles (estimated using the density of crystalline Li_2O_2[39]) alongside the total product volume formed (estimated based on mean particle size) and capacity at each rate. Although diameters of the disk-like particles appear to be roughly constant within error across the three slowest discharges, their heights vary with more significance.

Figure 6 shows how the discharge-product-particle volume, total number of particles, and particle surface-to-volume ratio

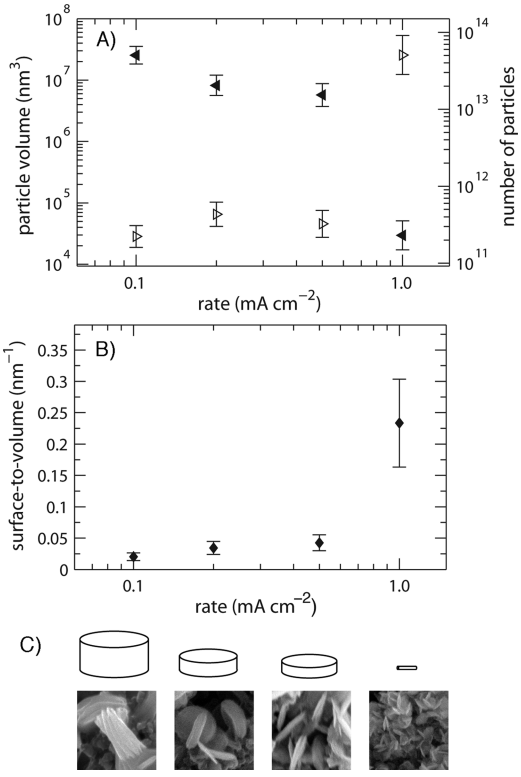

Figure 6. Particles decrease in volume but increase in surface area and number as rate increases. (A) Li_2O_2 particle volume (◀) and estimated total number of Li_2O_2 particles (▷) as functions of discharge rate. (B) Surface-to-volume ratio of discharge-product particles as a function of discharge rate. (C) Schematics of Li_2O_2 disks and needles with mean proportions drawn to scale, shown above SEM images for comparison.

vary with discharge rate, as well as providing schematic illustrations of the mean particle shapes, with relative sizes to scale. Estimates of the total numbers of particles based on the mean capacity and mean particle size correlate well with estimates of the total number of particles on the electrode surface computed using a direct measurement of particle surface density, suggesting that the structures seen on the surface likely contribute to the total capacity of the discharged cell. The total number of particles appears to rise super-exponentially as the discharge rate increases.

4. DISCUSSION

4.1. Macroscopic Diffusion Limitations. A significant body of research has addressed possible kinetic limitations to

Table 1. Variation of the Dimensions of Individual Li_2O_2 Particles and Cumulative Amount of Li_2O_2 Formed with Respect to the Discharge Current Density[a]

rate (mA cm^{-2})	particle diameter (nm)	particle height (nm)	particle volume (× 10^5 nm^3)	surface-to-volume ratio (× 10^{-2} nm^{-1})	number of particles (× 10^{12})	total product volume (mm^3)	discharge capacity (mAh cm^{-2})
0.1	415 ± 47	188 ± 44	254 ± 72	2.0 ± 0.5	0.22 ± 0.07	5.7 ± 0.9	6.0 ± 1.0
0.2	346 ± 41	88 ± 24	83 ± 26	3.4 ± 1.0	0.43 ± 0.16	3.6 ± 0.6	3.8 ± 0.6
0.5	334 ± 51	65 ± 19	57 ± 21	4.3 ± 1.4	0.33 ± 0.13	1.9 ± 0.4	2.0 ± 0.4
1.0	18.6 ± 4.8	109 ± 17	0.30 ± 0.12	23.3 ± 7.0	51 ± 29	1.5 ± 0.6	1.6 ± 0.7

[a]Number of particles and total product volume are estimated using the mean particle volume and the density of bulk crystalline Li_2O_2.

DOI: 10.1021/acsami.5b00574
ACS Appl. Mater. Interfaces 2015, 7, 7670−7678

Li_2O_2 formation.[31,40−42] The present electrochemical and morphology measurements suggest several factors besides reaction kinetics that could limit the performance of Li/O_2 cells, however. Performance limitations could owe in part to diffusive processes: although the importance of oxygen solubility and diffusivity in the liquid electrolyte has been recognized,[32] few efforts have been made to correlate these parameters with observed overpotentials and cell capacities.

Because the primary advantage of the Li/O_2 chemistry over Li-ion chemistry is its high specific energy, it is important that much of the capacity of the battery be available in response to all practical current demands. Figure 3 shows that the available capacity of the battery falls faster with rate than it does in other typical precipitation/dissolution battery systems, posing a design problem that merits close study: indeed, the Li/O_2 Peukert exponent of 1.6 ± 0.1 is even greater than the exponent of 1.4 for lead/acid cells,[34] whose poor rate performance is well known. Substantial transport limitations associated with oxygen could partially explain the rapid decrease in capacity with increasing current density in Li/O_2 cells. Because the cell reaction consumes molecular O_2, the rate of reaction in the porous positive electrode, determined by the current density, should always be balanced by the rate of oxygen diffusion through the pore-filling electrolyte. This diffusion rate is proportional to the oxygen permeability (the product of saturated O_2 concentration and effective O_2 diffusivity).

Because oxygen is more readily available near the gas reservoir, discharge-product formation should run to completion there first, consistent with the inhomogeneous spatial distribution of discharge products observed in neutron imaging of discharged electrodes.[25] Dissolved O_2 must subsequently diffuse through Li_2O_2-saturated domains at the rate demanded by the applied current. Given the extremely low O_2 solubility of DME,[32] and in light of typical O_2 diffusivities, the flux demanded by the discharge current can drive the O_2 concentration to vanish within a distance far smaller than the positive-electrode thickness.[22,25] "Sudden death" of voltage then occurs when the O_2 flux across the Li_2O_2-saturated domain cannot maintain the current density. Under the assumption that the capacity of the battery will be proportional to the distance that O_2 can penetrate into the positive electrode, the capacity would be expected to fall as a function of current with a Peukert exponent of 2, sufficiently close to the observed value of 1.6 ± 0.1 to suggest that macroscopic O_2 transport contributes to rate limitations.

Higher-order corrections owing to the discharge-product morphology could explain the fact that the observed Peukert exponent is somewhat smaller than 2. Under the hypothesis that O_2 transport plays a role in limiting discharge capacity, deviations from a Peukert exponent of 2 can be attributed to local changes in the O_2 permeability. Because the saturated O_2 concentration is a thermodynamic quantity, it is by definition rate-independent; thus, to rationalize the data, the effective O_2 diffusivity must be increasing somewhat with rate, even as the O_2 penetration depth is falling. Such an effect can be explained by observing that the effective diffusivity involves the electrode porosity and tortuosity. The SEM images show that the mean size of the Li_2O_2 particles at the lowest rate is comparable to the approximate size of the pores in the electrode (~350 nm). Therefore, at low rates, the effective O_2 diffusivity is decreased due to the lower porosity and much greater tortuosity of the diffusion path that O_2 must travel to reach unutilized pore volume deeper within the electrode. At the highest rate, the needle-like particles have volumes 2 to 3 orders of magnitude smaller than the disks. These needles occlude far less of the native pore structure of the carbon electrode, leading O_2 to have a higher effective diffusivity. This may explain why the Peukert exponent is dampened from the extreme value of 2.

To target better rate performance, the solubility and the effective diffusivity of oxygen in the positive electrode should be made as large as possible. A simple way to raise the oxygen solubility would be to raise the partial pressure of oxygen in the gas phase. McCloskey et al. show that this slightly reduces the overpotential for Li_2O_2 deposition but do not discuss the effect of a pressure increase on capacity in great detail.[42] Nemanick et al. have shown that the capacity increases with increasing pressure at a fixed discharged rate.[27]

4.2. Product Morphology. Discharge-product morphology can limit performance thermodynamically. Because the discharge products that form in the porous electrode comprise nanoscale particulates, a large surface-area change is incurred during discharge. A lowering of cell potential (i.e., an increase in apparent overpotential, or a reduction in apparent energy efficiency) could be associated with the surface-energy change incurred by creating Li_2O_2/electrolytic-solution and Li_2O_2/electrode interfacial areas at the expense of electrolytic-solution/electrode interfacial area.[43,44] The observed morphology differences among Li_2O_2 particles formed at different discharge rates raise more fundamental questions about the connection between the discharge mechanism of Li/O_2 cells and the cell voltage. The free energy needed to produce this large area could come at the expense of the potential delivered by the cell, reducing energy efficiency.

SEM images reported here and elsewhere[8,9,11,22] confirm that discharge-product shape is affected by the applied current, as well as thermodynamics. Supporting Information Figure S3 provides evidence for a lack of correlation between discharge-product morphology and capacity, as well as supporting a correlation between morphology and current. The rate processes that control particle morphology can be elucidated by examining Figure 6. Li_2O_2 formed at 0.1 mA cm^{-2} has a similar shape to the equilibrium Wulff constructions predicted in the literature,[45,46] although all but the {0001} faces appear to be roughened in the SEM images. The surface-to-volume ratios of the particles rise monotonically with rising discharge current; this trend supports the assertion that nonequilibrium energetics is a significant factor that determines product shapes. Mechanisms driven by supersaturation of a dissolved neutral intermediate or shape-dependent overpotential would both be consistent with the classical theory of nucleation and growth in electrodeposition.[43,47] The relationship among surface energy, growth rate, and morphology needs to be probed more deeply from a theoretical standpoint; some relevant work has been presented recently by Horstmann et al.[29]

Nonequilibrium surface energetics appears to control both the shapes and sizes of particles, as reflected by the changes in surface-to-volume ratio with current. Because the particle diameter was found to be relatively constant with respect to rate for the three lowest discharge currents, it appears that in the low-current limit, the growth perpendicular to the flat face is slowest in response to the overpotential, whereas growth perpendicular to the curved interface is sufficiently fast to reach its equilibrium curvature regardless of the local potential environment. At the highest current, however, the qualitative shape of the Li_2O_2 changes entirely, suggesting that the

DOI: 10.1021/acsami.5b00574
ACS Appl. Mater. Interfaces 2015, 7, 7670−7678

overpotential is sufficiently large that the curved interface also changes shape.

Adams et al.[8] reported a transition in discharge-product morphology to a thin film at high rates, but there was no evidence of such a transition in the present study, even though higher superficial current densities were investigated. Lu et al.[22] also explored a range of current densities, yet at the highest rate (0.76 mA cm^{-2} on a superficial-area basis) did not observe a thin discharge-product film. Differences in oxygen pressure, electrolyte composition, nature of the carbon support, and so forth could explain the different morphologies seen at high current densities. Nevertheless, it should be emphasized that averaging of many fast SEM scans was necessary to observe the presence of needle-like particles formed at 1 mA cm^{-2}. These Li_2O_2 particles have high surface-to-volume ratios and, therefore, are more susceptible to damage by the electron beam before their presence can be recorded; the remnants of beam damage could resemble a conformal film. The apparently conflicting data regarding the morphology of Li_2O_2 at high discharge rates suggest that additional study is needed to clarify the behavior in this important operating regime.

In the present work, XRD results serve primarily to ensure that most of the electrochemical and microscopic information can be attributed to the production of Li_2O_2. It remains, however, to consider the origins of the stria evident on particles formed at the lowest two rates (cf. Figure 5). XRD spectra show a characteristic crystallite size of about 20 nm that stays constant with respect to discharge rate, consistent with the spacing of the stria.

4.3. Product Growth Mechanisms. The exact means of charge transport through solid Li_2O_2 (if bulk Li_2O_2 supports any appreciable current at all) is still debated,[15,48] and the reaction pathway by which Li_2O_2 is created is also under discussion.[7,10,48−50] Data about the rate-dependent morphology and the distribution of Li_2O_2 are relevant to both topics.

At all rates, the particles observed with SEM exhibit at least one characteristic dimension that is too large for electron transport via tunneling.[48] A few alternative mechanisms for charge transport have been put forward to explain such large characteristic particle sizes. Adams et al.[20] suggest that the observed large particle sizes can be justified by a peroxide-formation mechanism that progresses through a LiO_2 intermediate, which may be soluble in the solution to an extent that allows it to react at the electrode and diffuse a significant distance before depositing as Li_2O_2. Some studies have proposed charge-conduction mechanisms by which electrons travel through amorphous Li_2O_2[16] or through crystalline Li_2O_2 along the surface,[17] along grain boundaries,[18] or through bulk defects.[15]

Two of the proposed mechanisms for the formation of Li_2O_2 are (i) reaction/dissolution, where soluble lithium superoxide forms at the pore surfaces within the electrodes, diffuses within pore-filling liquid, and reacts chemically to precipitate on peroxide surfaces[7] and (ii) an electrochemical deposition, where Li_2O_2 nucleates on the pore surface through a LiO_2 intermediate and propagates through additional charge exchange at the Li_2O_2 surface.[7] For the reaction/dissolution mechanism, a chemical deposition process involving neutral species would control the dimensions of the Li_2O_2 particles; in this case, the increase in surface-to-volume ratio with rate could be attributable to a higher supersaturation of the precipitating neutral species in the liquid phase when the intermediate is produced at higher rate or the surface-diffusion rate of those species on existing Li_2O_2 particles. Alternatively, if the particles form by an electrochemical process, the sizes and shapes of electrodeposits would be expected to change directly in response to the local kinetic overpotential; propagating particles tend to maximize the overpotential by increasing their surface-to-volume ratios, allowing higher rates of mass transfer to the electrodeposit by shortening the diffusion lengths of species in the liquid phase.[44] Thus, the observation of highly current-dependent morphology presented in Figure 5 supports the notions that either particle growth occurs by locally mass-transfer-limited processes (such as nucleation and growth by diffusion) involving neutral species or by a locally mass-transfer-limited electrochemical mechanism; either pathway can rationalize the significant variation in particle morphology as rate increases.

5. CONCLUSIONS

There is a growing awareness in the literature that the efficiency of the oxygen-evolution (charging) process in Li/O_2 batteries can depend on the structure of the phase that is being decomposed. To understand the high overpotentials typical of recharge, it is important to understand the morphology of the Li_2O_2 phase formed during the preceding discharge and how that morphology is affected by operating conditions. The present study aims to establish these relationships by quantifying how the average discharge capacity and product-particle morphology in Li/O_2 cells vary with the discharge current.

This investigation also clarifies several aspects of electrochemical experimental control. Systematic experiments were performed using porous positive electrodes without particulate additives, which were discharged at superficial current densities consistent with the needs for automotive applications. A steep decrease in discharge capacity with discharge rate was observed, supporting the notion that macroscopic transport processes control capacity in this current-density regime. When macroscopic transport is limiting, superficial current density likely correlates more strongly with discharge capacity than current densities normalized in other ways.

The measurement of a statistically significant Peukert exponent of 1.6 ± 0.1 also highlights the poor rate performance of state-of-the-art Li/O_2 cells in comparison to other precipitation/dissolution battery chemistries. The observed relationship between capacity and rate can be rationalized by a hypothesis that a lowering oxygen penetration depth in the positive electrode (decrease in electrode utilization) with increasing discharge rate is the dominant capacity-limiting factor.

SEM was performed using a novel air-free sample-transfer technique, which prevented samples from being exposed to air before vacuum was drawn in the microscope chamber. Performing many repeated independent first discharges allowed the characteristic dimensions of the Li_2O_2 particles formed during an average first discharge to be established with a high degree of statistical certainty. The Li_2O_2 was found to deposit as disks ("toroids") at lower rates, with a constant radius and a variable height; particles formed at lower rates appear to comprise stacked 20 nm layers of fixed diameter. Even at the highest rate, the discharge-product phase was observed to have a particulate, rather than a compact, structure. Needle-like shapes with very small characteristic dimensions form at 1 mA cm^{-2}. There is a stark difference in product morphology at the highest rate: the surface-to-volume ratio of the needles is an

DOI: 10.1021/acsami.5b00574
ACS Appl. Mater. Interfaces 2015, 7, 7670−7678

order of magnitude greater than the disks, and the number of needles formed is 2 orders of magnitude greater than the typical number of disks.

The surface-area-to-volume ratio of the discharge-product particles increases dramatically with increasing rate, suggesting that Li_2O_2 forms by a locally mass-transport-limited nucleation and growth mechanism. This is consistent with the notion that the interfacial energy of deposited Li_2O_2 varies with the discharge rate, either in response to the local overpotential environment or in response to the concentration fields of reactants or reactant intermediates.

■ ASSOCIATED CONTENT

Supporting Information

Open circuit relaxation data, SEM sample holder schematic, SEM images comparing morphology vs capacity and discharge rate. This material is available free of charge via the Internet at http://pubs.acs.org.

■ AUTHOR INFORMATION

Corresponding Author

*E-mail: cwmonroe@umich.edu.

Author Contributions

The manuscript was written through contributions of all authors. All authors have given approval to the final version of the manuscript.

Funding

This work was supported by Robert Bosch LLC through the Bosch Energy Research Network, grant no. 19.04.US11, and by the U.S. National Science Foundation, grant no. CBET-1336387.

Notes

The authors declare no competing financial interest.

■ ACKNOWLEDGMENTS

The authors gratefully acknowledge Dr. Paul Albertus for his valuable suggestions regarding the research.

■ REFERENCES

(1) Wagner, F. T.; Lakshmanan, B.; Mathias, M. F. Electrochemistry and the Future of the Automobile. *J. Phys. Chem. Lett.* **2010**, *1*, 2204−2219.

(2) Christensen, J.; Albertus, P.; Sanchez-Carrera, R. S.; Lohmann, T.; Kozinsky, B.; Liedtke, R.; Ahmed, J.; Kojic, A. A Critical Review of Li/Air Batteries. *J. Electrochem. Soc.* **2012**, *159*, R1−R30.

(3) Girishkumar, G.; McCloskey, B.; Luntz, A. C.; Swanson, S.; Wilcke, W. Lithium-Air Battery: Promise and Challenges. *J. Phys. Chem. Lett.* **2010**, *1*, 2193−2203.

(4) Lu, Y. C.; Gallant, B. M.; Kwabi, D. G.; Harding, J. R.; Mitchell, R. R.; Whittingham, M. S.; Shao-Horn, Y. Lithium-Oxygen Batteries: Bridging Mechanistic Understanding and Battery Performance. *Energy Environ. Sci.* **2013**, *6*, 750−768.

(5) Abraham, K. M.; Jiang, Z. A Polymer Electrolyte-Based Rechargeable Lithium/Oxygen Battery. *J. Electrochem. Soc.* **1996**, *143*, 1−5.

(6) McCloskey, B. D.; Bethune, D. S.; Shelby, R. M.; Girishkumar, G.; Luntz, A. C. Solvents' Critical Role in Nonaqueous Lithium-Oxygen Battery Electrochemistry. *J. Phys. Chem. Lett.* **2011**, *2*, 1161−1166.

(7) Peng, Z. Q.; Freunberger, S. A.; Hardwick, L. J.; Chen, Y. H.; Giordani, V.; Barde, F.; Novak, P.; Graham, D.; Tarascon, J. M.; Bruce, P. G. Oxygen Reactions in a Non-Aqueous Li^+ Electrolyte. *Angew. Chem., Int. Ed. Engl.* **2011**, *50*, 6351−6355.

(8) Adams, B. D.; Radtke, C.; Black, R.; Trudeau, M. L.; Zaghib, K.; Nazar, L. F. Current Density Dependence of Peroxide Formation in the Li−O_2 Battery and its Effect on Charge. *Energy Environ. Sci.* **2013**, *6*, 1772−1778.

(9) Gallant, B. M.; Kwabi, D. G.; Mitchell, R. R.; Zhou, J. G.; Thompson, C. V.; Shao-Horn, Y. Influence of Li_2O_2 Morphology on Oxygen Reduction and Evolution Kinetics in Li−O_2 Batteries. *Energy Environ. Sci.* **2013**, *6*, 2518−2528.

(10) Leskes, M.; Moore, A. J.; Goward, G. R.; Grey, C. P. Monitoring the Electrochemical Processes in the Lithium-Air Battery by Solid State NMR Spectroscopy. *J. Phys. Chem. C* **2013**, *117*, 26929−26939.

(11) Mitchell, R. R.; Gallant, B. M.; Thompson, C. V.; Shao-Horn, Y. All-Carbon-Nanofiber Electrodes for High-Energy Rechargeable Li-O2 Batteries. *Energy Environ. Sci.* **2011**, *4*, 2952−2958.

(12) Xu, D.; Wang, Z. L.; Xu, J. J.; Zhang, L. L.; Zhang, X. B. Novel DMSO-Based Electrolyte for High Performance Rechargeable Li−O_2 Batteries. *Chem. Commun.* **2012**, *48*, 6948−6950.

(13) Xu, J. J.; Wang, Z. L.; Xu, D.; Zhang, L. L.; Zhang, X. B. Tailoring Deposition and Morphology of Discharge Products Towards High-Rate and Long-Life Lithium-Oxygen Batteries. *Nat. Commun.* **2013**, *4*, 2438.

(14) Xia, C.; Waletzko, M.; Chen, L.; Peppler, K.; Klar, P. J.; Janek, J. Evolution of Li_2O_2 Growth and its Effect on Kinetics of Li−O_2 Batteries. *ACS Appl. Mater. Interfaces* **2014**, *6*, 12083−12092.

(15) Radin, M. D.; Siegel, D. J. Charge Transport in Lithium Peroxide: Relevance for Rechargeable Metal-Air Batteries. *Energy Environ. Sci.* **2013**, *6*, 2370−2379.

(16) Tian, F.; Radin, M. D.; Siegel, D. J. Enhanced Charge Transport in Amorphous Li_2O_2. *Chem. Mater.* **2014**, *26*, 2952−2959.

(17) Radin, M. D.; Rodriguez, J. F.; Tian, F.; Siegel, D. J. Lithium Peroxide Surfaces are Metallic, While Lithium Oxide Surfaces are Not. *J. Am. Chem. Soc.* **2011**, *134*, 1093−1103.

(18) Geng, W. T.; He, B. L.; Ohno, T. Grain Boundary Induced Conductivity in Li_2O_2. *J. Phys. Chem. C* **2013**, *117*, 25222−25228.

(19) Yilmaz, E.; Yogi, C.; Yamanaka, K.; Ohta, T.; Byon, H. R. Promoting Formation of Noncrystalline Li_2O_2 in the Li−O_2 Battery with RuO_2 Nanoparticles. *Nano Lett.* **2013**, *13*, 4679−4684.

(20) Adams, J.; Karulkar, M.; Anandan, V. Evaluation and Electrochemical Analyses of Cathodes for Lithium-Air Batteries. *J. Power Sources* **2013**, *239*, 132−143.

(21) USABC Goals for Advanced Batteries for EVs. http://www.uscar.org/guest/teams/12/U-S-Advanced-Battery-Consortium (accessed Jan 2015).

(22) Lu, Y. C.; Kwabi, D. G.; Yao, K. P.; Harding, J. R.; Zhou, J.; Zuin, L.; Shao-Horn, Y. The Discharge Rate Capability of Rechargeable Li−O_2 Batteries. *Energy Environ. Sci.* **2011**, *4*, 2999−3007.

(23) Jung, H. G.; Hassoun, J.; Park, J.-B.; Sun, Y.-K.; Scrosati, B. An Improved High-Performance Lithium−Air Battery. *Nat. Chem.* **2012**, *4*, 579−585.

(24) Peukert, Über die Abhängigkeit der Kapazität von der Entladestromstärke bei Bleiakkumulatoren. *ETZ, Elektrotech. Z., Ausg. A* **1897**, *18*, 20−21.

(25) Nanda, J.; Bilheux, H.; Voisin, S.; Veith, G. M.; Archibald, R.; Walker, L.; Allu, S.; Dudney, N. J.; Pannala, S. Anomalous Discharge Product Distribution in Lithium-Air Cathodes. *J. Phys. Chem. C* **2012**, *116*, 8401−8408.

(26) Jung, H. G.; Kim, H.-S.; Park, J.-B.; Oh, I.-H.; Hassoun, J.; Yoon, C. S.; Scrosati, B.; Sun, Y.-K. A Transmission Electron Microscopy Study of the Electrochemical Process of Lithium/Oxygen Cells. *Nano Lett.* **2012**, *12*, 4333−4335.

(27) Nemanick, E. J.; Hickey, R. P. The Effects of O_2 Pressure on Li−O_2 Secondary Battery Discharge Capacity and Rate Capability. *J. Power Sources* **2014**, *252*, 248−251.

(28) Meini, S.; Piana, M.; Beyer, H.; Schwämmlein, J.; Gasteiger, H. A. Effect of Carbon Surface Area on First Discharge Capacity of Li−O_2 Cathodes and Cycle-Life Behavior in Ether-Based Electrolytes. *J. Electrochem. Soc.* **2012**, *159*, A2135−A2142.

DOI: 10.1021/acsami.5b00574
ACS Appl. Mater. Interfaces 2015, 7, 7670−7678

(29) Horstmann, B.; Gallant, B.; Mitchell, R.; Bessler, W. G.; Shao-Horn, Y.; Bazant, M. Z. Rate-Dependent Morphology of Li_2O_2 Growth in Li−O_2 Batteries. *J. Phys. Chem. Lett.* **2013**, *4*, 4217−4222.
(30) Viswanathan, V.; Nørskov, J. K.; Speidel, A.; Scheffler, R.; Gowda, S.; Luntz, A. C. Li−O_2 Kinetic Overpotentials: Tafel Plots from Experiment and First-Principles Theory. *J. Phys. Chem. Lett.* **2013**, *4*, 556−560.
(31) Lu, Y. C.; Gasteiger, H. A.; Shao-Horn, Y. Catalytic Activity Trends of Oxygen Reduction Reaction for Nonaqueous Li-Air Batteries. *J. Am. Chem. Soc.* **2011**, *133*, 19048−19051.
(32) Read, J.; Mutolo, K.; Ervin, M.; Behl, W.; Wolfenstine, J.; Driedger, A.; Foster, D. Oxygen Transport Properties of Organic Electrolytes and Performance of Lithium/Oxygen Battery. *J. Electrochem. Soc.* **2003**, *150*, A1351−A1356.
(33) Baert, D.; Vervaet, A. Lead-Acid Battery Model for the Derivation of Peukert's Law. *Electrochim. Acta* **1999**, *44*, 3491−3504.
(34) Gillibrand, M. I.; Lomax, G. R. The Discharge Characteristics of Lead-Acid Battery Plates. *Electrochim. Acta* **1963**, *8*, 693−702.
(35) Omar, N.; Verbrugge, B.; Mulder, G.; Van den Bossche, P.; Van Mierlo, J.; Daowd, M.; Dhaens, M.; Pauwels, S. Evaluation of Performance Characteristics of Various Lithium-Ion Batteries for Use in BEV Application. *Vehicle Power and Propulsion Conference (VPPC)*; IEEE: New York, 2010; pp 1−6.
(36) Dubarry, M.; Truchot, C.; Cugnet, M.; Liaw, B. Y.; Gering, K.; Sazhin, S.; Jamison, D.; Michelbacher, C. Evaluation of Commercial Lithium-Ion Cells Based on Composite Positive Electrode for Plug-In Hybrid Electric Vehicle Applications. Part I: Initial Characterizations. *J. Power Sources* **2011**, *196*, 10328−10335.
(37) Veith, G. M.; Dudney, N. J.; Howe, J.; Nanda, J. Spectroscopic Characterization of Solid Discharge Products in Li/Air Cells With Aprotic Carbonate Electrolytes. *J. Phys. Chem. C* **2011**, *115*, 14325−14333.
(38) McCloskey, B. D.; Speidel, A.; Scheffler, R.; Miller, D. C.; Viswanathan, V.; Hummelshoj, J. S.; Norskov, J. K.; Luntz, A. C. Twin Problems of Interfacial Carbonate Formation in Nonaqueous Li−O_2 Batteries. *J. Phys. Chem. Lett.* **2012**, *3*, 997−1001.
(39) *CRC Handbook of Chemistry*, 95th ed.; Haynes, W. M., Ed.; CRC Press: Boca Raton, FL, 2014; http://www.hbcpnetbase.com.
(40) Debart, A.; Bao, J.; Armstrong, G.; Bruce, P. G. An O_2 Cathode for Rechargeable Lithium Batteries: the Effect of a Catalyst. *J. Power Sources* **2007**, *174*, 1177−1182.
(41) McCloskey, B. D.; Scheffler, R.; Speidel, A.; Bethune, D. S.; Shelby, R. M.; Luntz, A. C. On the Efficacy of Electrocatalysis in Nonaqueous Li−O_2 Batteries. *J. Am. Chem. Soc.* **2011**, *133*, 18038−18041.
(42) McCloskey, B. D.; Scheffler, R.; Speidel, A.; Girishkumar, G.; Luntz, A. C. On the Mechanism of Nonaqueous Li−O_2 Electrochemistry on C and its Kinetic Overpotentials: Some Implications for Li-Air Batteries. *J. Phys. Chem. C* **2012**, *116*, 23897−23905.
(43) Diggle, J. W.; Despic, A. R.; Bockris, J. O. The Mechanism of the Dendritic Electrocrystallization of Zinc. *J. Electrochem. Soc.* **1969**, *116*, 1503−1514.
(44) Monroe, C.; Newman, J. The Effect of Interfacial Deformation on Electrodeposition Kinetics. *J. Electrochem. Soc.* **2004**, *151*, A880−A886.
(45) Mo, Y.; Ong, S. P.; Ceder, G. First-Principles Study of the Oxygen Evolution Reaction of Lithium Peroxide in the Lithium-Air Battery. *Phys. Rev. B: Condens. Matter Mater. Phys.* **2011**, *84*, 205446.
(46) Radin, M. D.; Tian, F.; Siegel, D. J. Electronic Structure of Li_2O_2 {0001} Surfaces. *J. Mater. Sci.* **2012**, *47*, 7564−7570.
(47) Barton, J. L.; Bockris, J. O. Electrolytic Growth of Dendrites from Ionic Solutions. *Proc. R. Soc. London, Ser. A* **1962**, *268*, 485.
(48) Viswanathan, V.; Thygesen, K. S.; Hummelshoj, J. S.; Norskov, J. K.; Girishkumar, G.; McCloskey, B. D.; Luntz, A. C. Electrical Conductivity in Li_2O_2 and its Role in Determining Capacity Limitations in Non-Aqueous Li−O_2 Batteries. *J. Chem. Phys.* **2011**, *135*, 214704.
(49) Laoire, C. O.; Mukerjee, S.; Abraham, K. M.; Plichta, E. J.; Hendrickson, M. A. Influence of Nonaqueous Solvents on the Electrochemistry of Oxygen in the Rechargeable Lithium-Air Battery. *J. Phys. Chem. C* **2010**, *114*, 9178−9186.
(50) Xu, W.; Xu, K.; Viswanathan, V. V.; Towne, S. A.; Hardy, J. S.; Xiao, J.; Hu, D. H.; Wang, D. Y.; Zhang, J. G. Reaction Mechanisms for the Limited Reversibility of Li−O_2 Chemistry in Organic Carbonate Electrolytes. *J. Power Sources* **2011**, *196*, 9631−9639.

NOTE ADDED AFTER ASAP PUBLICATION

This paper published ASAP on April 1, 2015. The TOC/Abstract image was replaced and the revised version was reposted on April 6, 2015.

DOI: 10.1021/acsami.5b00574
ACS Appl. Mater. Interfaces 2015, 7, 7670−7678